Research Article

Cancer Immunology Research

FAP Delineates Heterogeneous and Functionally Divergent Stromal Cells in Immune-Excluded Breast Tumors

Viviana Cremasco[1], Jillian L. Astarita[1], Angelo L. Grauel[1], Shilpa Keerthivasan[2], Kenzie MacIsaac[3], Matthew C. Woodruff[4,5], Michael Wu[1], Lotte Spel[1], Stephen Santoro[2], Zohreh Amoozgar[1], Tyler Laszewski[3], Sara Cruz Migoni[6], Konstantin Knoblich[6,7], Anne L. Fletcher[6,7], Martin LaFleur[1], Kai W. Wucherpfennig[1], Ellen Pure[8], Glenn Dranoff[3], Michael C. Carroll[4,9], and Shannon J. Turley[1,10]

Abstract

Cancer-associated fibroblasts (CAFs) are generally associated with poor clinical outcome. CAFs support tumor growth in a variety of ways and can suppress antitumor immunity and response to immunotherapy. However, a precise understanding of CAF contributions to tumor growth and therapeutic response is lacking. Discrepancies in this field of study may stem from heterogeneity in the composition and function of fibroblasts in the tumor microenvironment. Furthermore, it remains unclear whether CAFs directly interact with and suppress T cells. Here, mouse and human breast tumors were used to examine stromal cells expressing fibroblast activation protein (FAP), a surface marker for CAFs. Two discrete populations of FAP^+ mesenchymal cells were identified on the basis of podoplanin (PDPN) expression: a FAP^+PDPN^+ population of CAFs and a FAP^+PDPN^- population of cancer-associated pericytes (CAPs). Although both subsets expressed extracellular matrix molecules, the CAF transcriptome was enriched in genes associated with TGFβ signaling and fibrosis compared with CAPs. In addition, CAFs were enriched at the outer edge of the tumor, in close contact with T cells, whereas CAPs were localized around vessels. Finally, FAP^+PDPN^+ CAFs suppressed the proliferation of T cells in a nitric oxide–dependent manner, whereas FAP^+PDPN^- pericytes were not immunosuppressive. Collectively, these findings demonstrate that breast tumors contain multiple populations of FAP-expressing stromal cells of dichotomous function, phenotype, and location. *Cancer Immunol Res; 6(12); 1472–85. ©2018 AACR.*

Introduction

Cancer-associated fibroblasts (CAFs) are the predominant nonhematopoietic stromal cell type in tumors, and their abundance often correlates with poor prognosis (1–4). Several roles have been ascribed to CAFs, including production of tumor mitogenic factors, deposition of extracellular matrix (ECM), stimulation of angiogenesis (5–7), and even immune cell trafficking and activation (5). Targeting fibroblast activation protein (FAP) to eradicate CAFs has demonstrated that a reduction in fibroblasts decreased collagen content and tumor burden (8–12), improving the effectiveness of immunotherapy (13, 14). Similarly, abrogation of CXCL12 produced by FAP^+ cells synergized with PD-L1 blockade to control the growth of pancreatic cancer in mice (13). Whether CAFs suppress the function of tumor-infiltrating T cells through direct or indirect mechanisms remains unclear.

One of the factors that have limited our understanding of how CAFs modulate antitumor immunity is a lack of specific markers to identify CAFs. FAP, for example, is expressed by some tumor-infiltrating immune cells (14, 15) and is also expressed in lymph nodes (LN; refs. 16, 17). Similarly, expression of alpha-smooth muscle actin (αSMA), another putative fibroblast-specific marker (18–20), is detected in other stromal cells. Another limitation is represented by a dearth of techniques to freshly isolate low-abundance stromal cells with high

[1]Department of Cancer Immunology and AIDS, Dana-Farber Cancer Institute, Boston, Massachusetts. [2]Genentech, South San Francisco, California. [3]Novartis Institutes for BioMedical Research, Cambridge, Massachusetts. [4]Program in Cellular and Molecular Medicine, Children's Hospital, Boston, Massachusetts. [5]Division of Medical Sciences, Harvard Medical School, Boston, Massachusetts. [6]Institute of Immunology and Immunotherapy, University of Birmingham, Edgbaston, United Kingdom. [7]Biomedicine Discovery Institute, Monash University, Clayton, Victoria, Australia. [8]Department of Biomedical Sciences, University of Pennsylvania School of Veterinary Medicine, Philadelphia, Pennsylvania. [9]Department of Pediatrics, Harvard Medical School, Boston, Massachusetts. [10]Department of Microbiology and Immunobiology, Harvard Medical School, Boston, Massachusetts.

Note: Supplementary data for this article are available at Cancer Immunology Research Online (http://cancerimmunolres.aacrjournals.org/).

V. Cremasco and J. Astarita contributed equally to this article.

Current address for V. Cremasco and A.L. Grauel: Novartis Institutes for BioMedical Research, Cambridge, Massachusetts; and current address J.L. Astarita and S.J. Turley: Genentech, South San Francisco, California.

Corresponding Authors: Shannon J. Turley, Genentech Inc., 1 DNA Way, South San Francisco, CA 94080. Phone: 650-225-2790; Fax: 650-742-1580; E-mail: turley.shannon@gene.com; and Viviana Cremasco, Novartis, 250 Massachusetts Ave., Cambridge, MA 02139. Phone: 617-871-4721; Fax: 617-871-4714; E-mail: viviana.cremasco@novartis.com

doi: 10.1158/2326-6066.CIR-18-0098

viability and reproducibility from tumors. Furthermore, the potential heterogeneity within CAFs adds complexity to the issue of fibroblast identification (21, 22).

We developed a protocol to isolate mouse and human stromal cells from tumors, which enabled the identification of two FAP^+ stromal subsets differentiated by the expression of the glycoprotein podoplanin (PDPN). FAP^+PDPN^+ cells expressed canonical fibroblast genes and exhibited some resemblance to fibroblasts of LNs, including the ability to construct a reticular network of fibers and secrete chemokines (23, 24), which engenders interactions of tumor-infiltrating lymphocytes and stromal cells. The $PDPN^-$ subset of FAP^+ cells was identified as cancer-associated pericytes ($PDPN^-$ CAPs), as confirmed by their localization around vasculature. Functionally, $PDPN^+$ CAFs suppressed T-cell proliferation through nitric oxide (NO) production, whereas $PDPN^-$ CAPs had no effect on T-cell proliferation.

Taken together, our study highlights heterogeneity within FAP^+ tumor mesenchymal cells, identifying nitric oxide as a stromal mediator of immunosuppression.

Materials and Methods

Mice and tumor models

Sex-matched BALB/c and C57BL/6 mice were purchased from The Jackson Laboratory. Mice were maintained under specific pathogen-free conditions in accordance with institutional guidelines and guidelines of the U.S. National Institutes of Health and were used at 5 to 7 weeks of age. B16, EL4, 4T1, A20, MC38, and CT26 WT cells were obtained from American Type Culture Collection. Pan02 cells were obtained from the NCI Developmental Therapeutics Program repository. The 4T07 cells were obtained from Dr. J. Lieberman (Harvard University, Cambridge, MA). Cells were maintained in Dulbecco's Modified Eagle Medium (B16, MC38, and EL4) or RPMI (4T1, A20, Pan02, CT26, and 4T07) supplemented with 10% FBS and penicillin/streptomycin and were not used for more than 10 passages after they were obtained in 2012. All cells were *mycoplasma* free but were not authenticated in the past year. For tumor inoculation, cells were detached using 0.25% trypsin, resuspended in PBS, and 1×10^5 to 1×10^6 cells were implanted subcutaneously on the upper-right dorsal flank of naïve recipient mice (4T1, 4T07, CT26, and A20 into BALB/c mice; B16, MC38, EL4, and Pan02 into C57BL/6 mice). Mice were monitored for tumor growth and body condition and were euthanized when tumor size reached 0.5 to 1 cm diameter. For orthotopic tumor studies, 1×10^6 cells 4T1 cells were injected into the mammary fat pad. All animal studies were approved by the Research Animal Care Committee of Dana-Farber Cancer Institute and Genentech.

Human samples

Human breast tissue samples for flow cytometry analysis were obtained from The MT Group. Primary human CAFs from breast carcinomas (CAF06) were obtained from Vitro-Biopharma and maintained in low-serum MSC-GroTM media as per company's instructions.

Tissue digestion for stromal cell isolation

Tumors were minced into fine pieces (approximately 1 mm^3) using scissors and razor blades, transferred into 15 mL conical tubes containing 2 mL of digestion buffer [RPMI (Gibco), 2% FBS, 0.2 mg/mL Collagenase P (Roche), 0.2 mg/mL Dispase (Gibco), and 0.1 mg/mL DNase I (Roche)], and placed into a water bath at 37°C. The tubes were vortexed every 5 minutes for 15 minutes, the tissue pieces were allowed to settle for 5 minutes, and then the supernatant containing freed cells was collected and quenched at 4°C in 50 mL conical tubes containing 20 mL of cold flow cytometry buffer (PBS, 2% FBS, and 2 mmol/L EDTA). Next, 2 mL of fresh digestion buffer was added to the remaining tumor fragments, and tubes were incubated at 37°C for another 20 minutes, vortexing every 5 minutes, prior to collecting the freed cells and adding them to the previously collected fractions on ice. These 20 minute digestion cycles were repeated for a total of 5 to 6 times, with progressively more forceful agitation methods (vortexing, pipetting 1 mL up and down using large orifice tips, then mixing with uncut 1 mL tips), until no tumor fragments larger than 1 mm remained. The collection tube containing the digested fractions in flow cytometry buffer was kept on ice until the digestion was complete, and then the contents was filtered through 70-μm mesh, centrifuged (1500 rpm, 10 minutes, 4°C), and the cells were counted. Pellets were resuspended in flow cytometry buffer or medium and subjected to immunostaining or *in vitro* assays. Skin fibroblasts were isolated from the flank of naïve, age-matched mice using the same procedure indicated above for tumors, but with a higher (5×) concentration of collagenase P in the digestion buffer. FRCs were isolated from skin-draining LNs as previously described (25).

Antibodies and reagents

For flow cytometry and imaging studies with murine tissues, the following antibodies were purchased from BioLegend: anti-CD45 (30-F11), anti-CD31 (390), anti-PDPN (8.1.1), anti-α-smooth muscle actin (1A4), anti-Thy1 (53-2.1), anti-CD140α (APA5), anti-CD140b (APB5), anti-CD106 (429), anti-CD4 (RM4.5), and anti-CD8 (RM2206). The anti-FAP used for flow cytometry analysis was provided by Ellen Pure and has been validated (anti-mouse FAP 73.3; ref. 8). For immunofluorescent analysis, the Roche anti-FAP 28H1 clone was used (26). Functional-grade purified anti-CD3ε (145-2C11) was obtained from BD Biosciences, and anti-CD28 (37.51) was from BioLegend. Antibodies used to stain human samples include viability dye (L10119; Life Technologies), anti-PDPN (clone NZ1.3; eBioscience), anti-Thy1 (clone 5E10; BD Biosciences), anti-CD4 (clone A161A1; BioLegend), and anti-CD8 (clone HIT8α; BioLegend). For PBMC stimulation, anti-human CD3 (clone OKT3; eBioscience) and anti-human CD28 (clone CD28.2; eBioscience) were used. L-NMMA (NG-monomethyl-L-arginine) was purchased from Calbiochem and CFSE (carboxyfluorescein diacetate succinimidyl ester) was from Invitrogen.

Microscopic analysis

Isolated tissues were fixed for 2 to 4 hours at room temperature in 4% paraformaldehyde (PFA) in PBS and then transferred to 30% sucrose to saturate overnight. Tissues were embedded in optimal cutting temperature medium (Sakura Finetek) and frozen for storage at −80°C. Next, 10- to 20-μm thick sections were cut on a cryostat, immunostained, and imaged with a Leica SP5X laser-scanning confocal microscope. Alternatively, fixed tumors were serially cut in 100-μm thick sections, imaged by multiphoton microscopy and assembled using Imaris software (Bitplane) to

enable digital reconstruction. Final analysis was performed using Volocity image analysis software (PerkinElmer).

Flow cytometry analysis

Tumor single-cell suspensions were resuspended in flow cytometry buffer (PBS, 2% FBS, and 2 mmol/L EDTA), blocked with Fc block, and then stained with different fluorochrome-conjugated antibodies for 15 minutes on ice. Samples were run on a BD flow cytometry Aria II and analyzed with FlowJo.

Cell enrichment and sorting

Single-cell suspensions prepared as described above were stained with biotinylated antibodies against CD45, CD31, CD49b, and Ter119, and negative cells were collected using the EasySep biotin selection kit according to the manufacturer's instructions. After enrichment, cells were stained and sorted on a BD flow cytometry ARIA II (100-μm nozzle, 20 psi). Dead cells were excluded using propidium iodide (5 ng/mL). Purity was assessed every time by sorting some cells into PBS and immediately reanalyzing them.

Microarray analysis

Cells were sorted into TRIzol, and RNA was prepared according to the guidelines of the Immunological Consortium. Isolated RNA was amplified and hybridized to the Affimetrix Mouse Gene 1.0 ST array. Normalized data were $\log_2$ transformed, row-centered, and clustered using the hierarchical clustering module of GenePattern and displayed using the heat map image module (www.genepattern.com).

Coculture of T cells and stromal cells

Freshly sorted 4T1 PDPN$^+$ CAFs, 4T1 PDPN$^-$ CAPs, or LN FRCs were plated in 96-well plates (5×10^4 cells per well) and allowed to adhere overnight. The next day, CFSE-labeled splenocytes (1×10^6) were added to the plates, together with soluble anti-CD3 (0.25 μg/mL) and anti-CD28 (0.25 μg/mL), and cultures were analyzed by flow cytometry 24 to 72 hours later. For experiments with human cells, 2.5×10^5 crystal violet–labeled PBMCs from anonymous healthy donors were plated with 5×10^4 CAFs and activated with anti-CD3 (2 μg/mL) and anti-CD28 (1 μg/mL) for 72 hours.

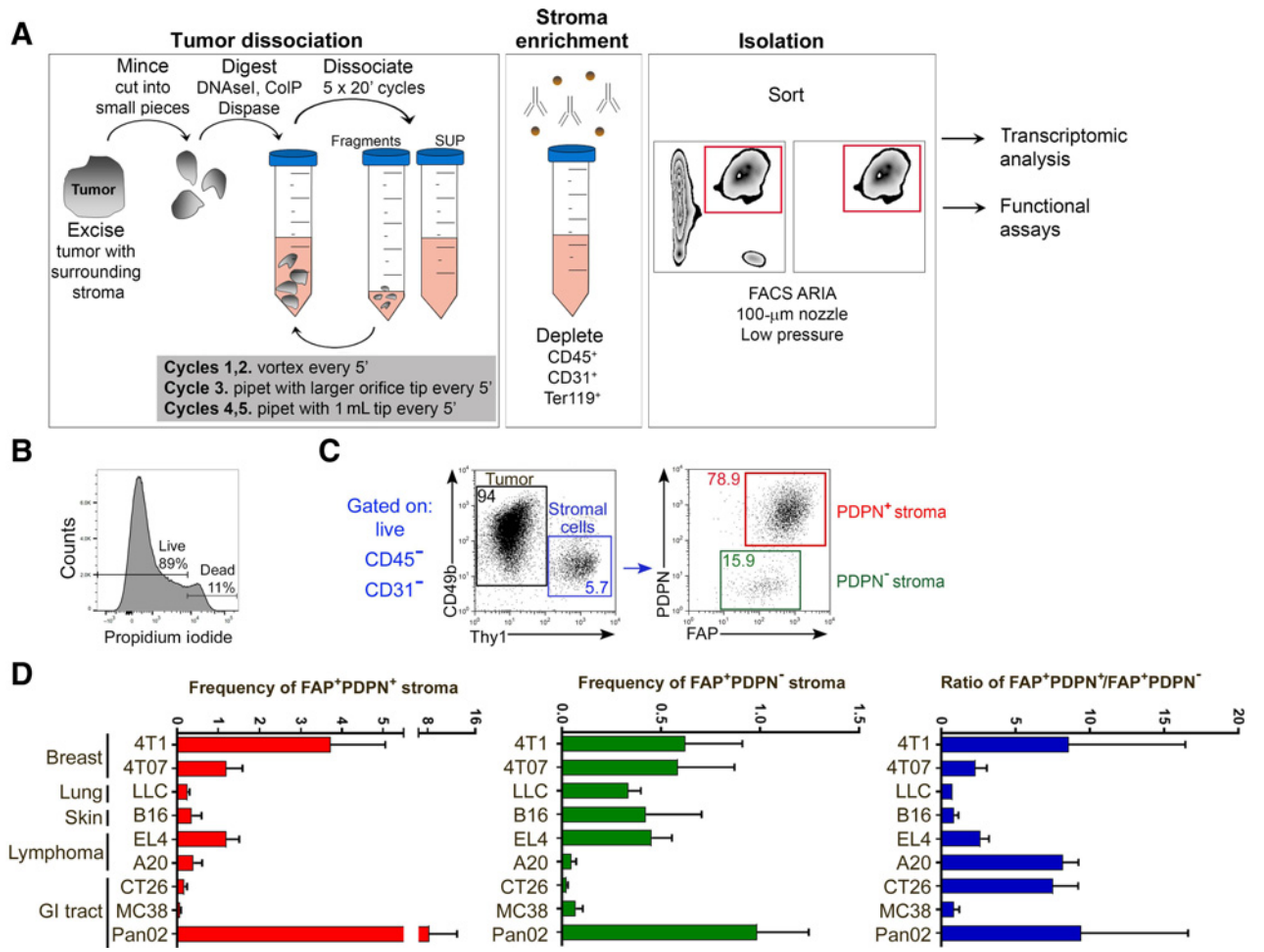

Figure 1.

Isolation of tumor mesenchymal stromal cells reveals heterogeneity within the FAP$^+$ compartment. **A,** Schematic depicting tumor stromal cell digestion and preparation. **B,** Representative plot showing viability of single-cell suspensions after tissue digestion. **C,** Representative flow-cytometric profile of s.c. 4T1 tumor single-cell suspensions. The FAP$^+$ PDPN$^+$ (PDPN$^+$ stroma, in red) and FAP$^+$ PDPN$^-$ (PDPN$^-$ stroma, in green) populations are highlighted. **D,** Frequencies of FAP$^+$ PDPN$^+$ and FAP$^+$ PDPN$^-$ cells in various subcutaneously implanted murine syngeneic tumors (percentage of total cellularity), and the ratio of FAP$^+$ PDPN$^+$ and FAP$^+$ PDPN$^-$ cells in these tumors. $N = 2$–7 independent experiments per model. Data are expressed as mean ± standard deviation.

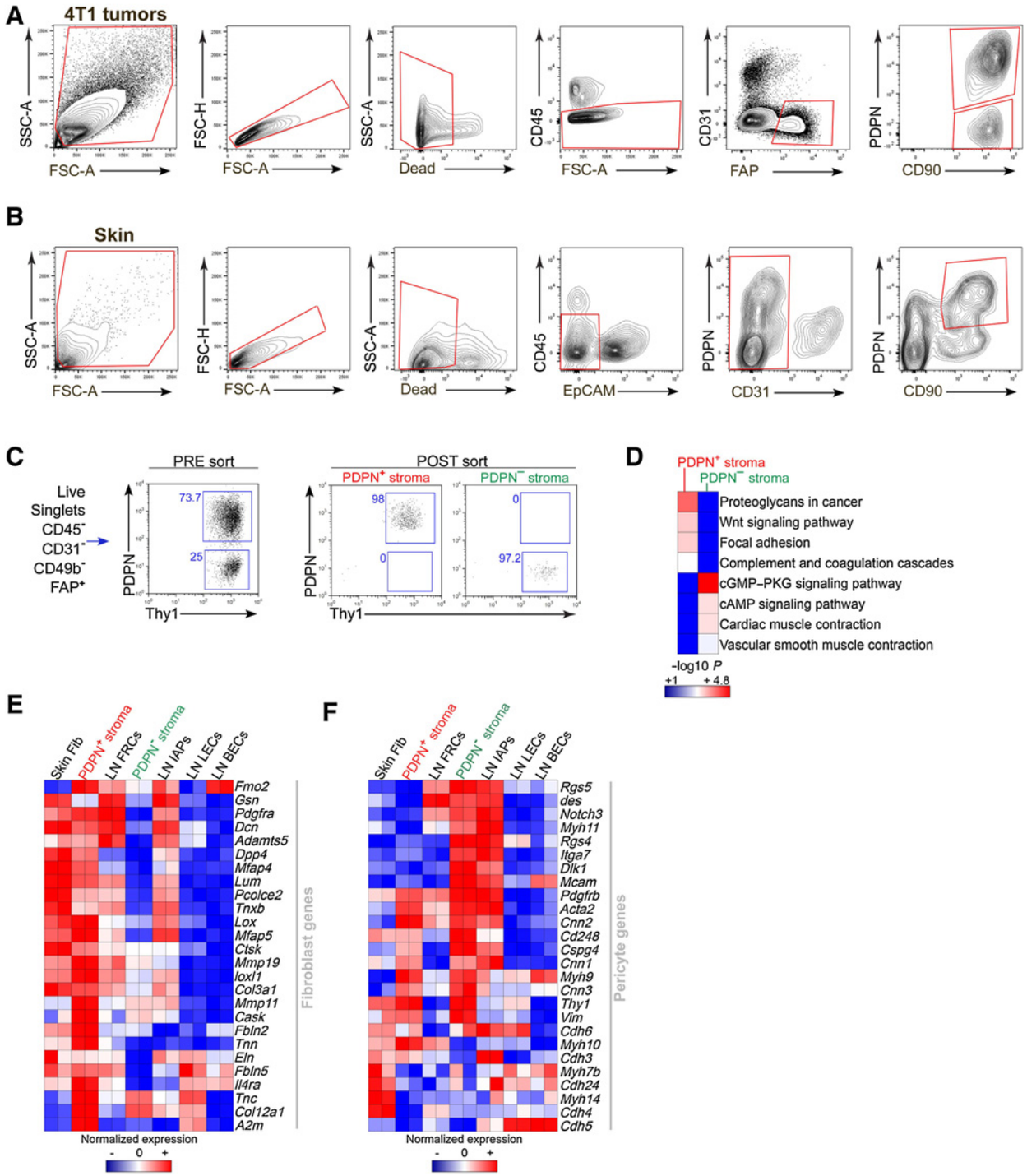

Figure 2.

Transcriptomic analysis of FAP$^+$ cell populations. **A** and **B,** Representative gating strategy for 4T1 tumor stroma (**A**) and skin fibroblasts (**B**). **C,** Representative sort strategy and post-sort FACS analysis for PDPN$^+$ and PDPN$^-$ stromal subsets from 4T1 tumors. Numbers indicate frequencies. **D,** The top 100 differentially expressed genes between PDPN$^+$ and PDPN$^-$ stromal subsets were analyzed for pathway enrichment (KEGG) using the DAVIS database. **E** and **F,** Expression of fibroblast (**E**) and pericyte (**F**) canonical genes was determined in PDPN$^+$ and PDPN$^-$ stromal subsets and compared with skin fibroblasts and LN stromal cells. (Skin Fib, skin fibroblasts; Tum PDPN$^+$, tumor FAP$^+$PDPN$^+$ stroma; LN FRCs, lymph node fibroblastic reticular cells; Tum PDPN$^-$, tumor FAP$^+$PDPN$^-$ stroma; LN IAPs, lymph node integrin $\alpha7^+$ pericytes; LN LECs, lymph node lymphatic endothelial cells; LN BECs, lymph node blood endothelial cells.) Heat maps show hierarchical clustering for probes with EV>120 for at least one population. Values were normalized, row mean centered, and $\log_2$ transformed.

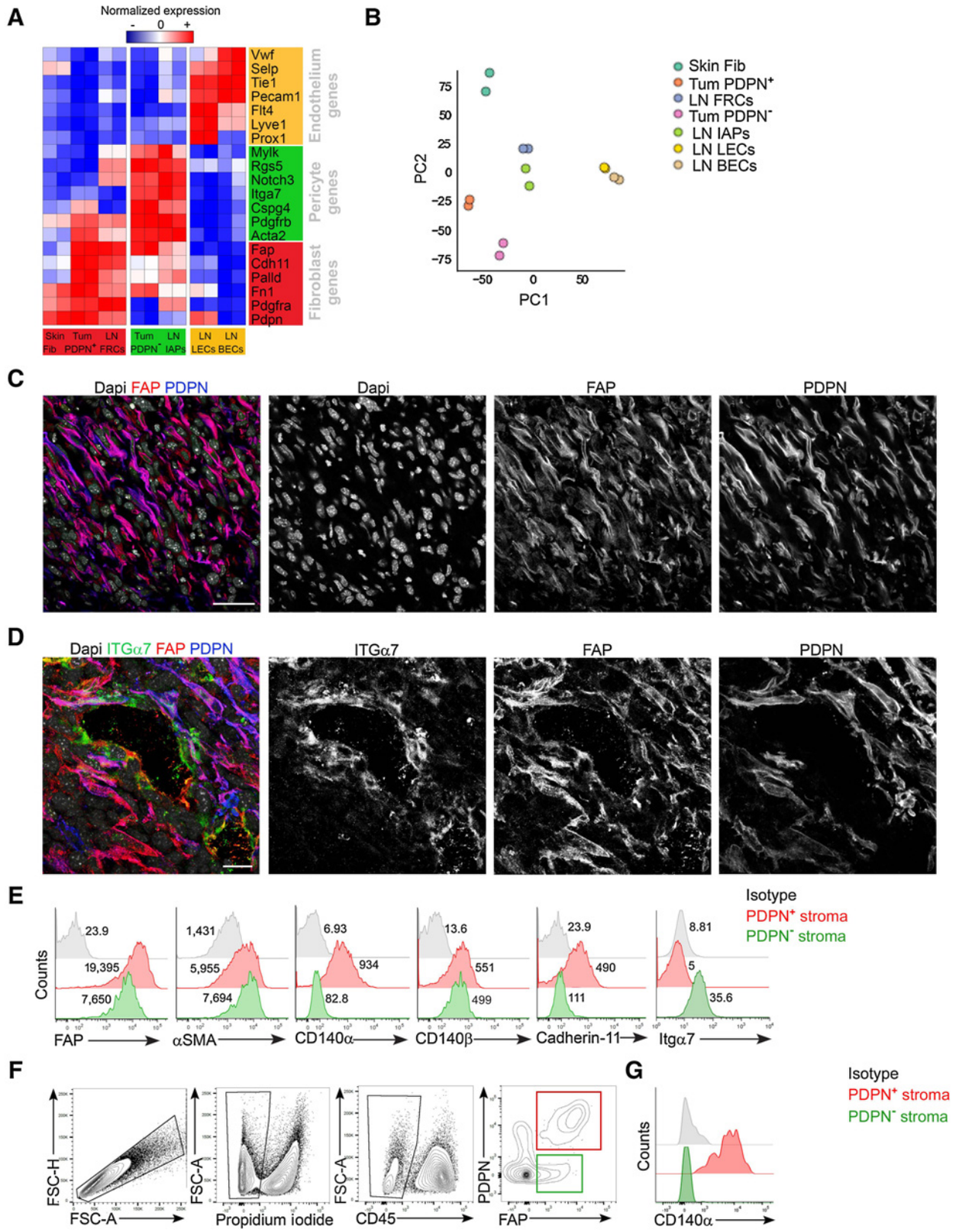

Measurement of NO production

The concentration of NO in cell culture supernatants was determined using the Griess reagent system (Promega), according to the manufacturer's instructions.

Statistical analysis

Two-tailed, unpaired Student *t* tests were used for statistical analyses, with the assumption of equal sample variance, with GraphPad Prism software. Differences with a P value of <0.05 were considered statistically significant.

Results

Tumor stroma heterogeneity within the FAP$^+$ compartment

In order to reproducibly isolate CAFs from primary tumors, we adapted a protocol that we had previously optimized to extract stromal cells from LNs (25). Using a combination of physical and enzymatic dissociation (Fig. 1A), stromal cells were released from transplanted murine syngeneic tumors, with viability greater than 90% (Fig. 1B). To examine the mesenchymal component of tumors, single-cell suspensions were stained with a FAP-specific antibody, together with a panel of antibodies against lineage markers to exclude hematopoietic cells (CD45), 4T1 tumor cells (CD49b; Supplementary Fig. S1A), and endothelial cells (CD31). The mesenchymal marker, Thy1 (27), and podoplaninin (PDPN), a glycoprotein expressed by fibroblasts from a variety of tissues (28), were also evaluated. Mesenchymal tumor components were identified by high expression of FAP and Thy1, and the absence of hematopoietic, endothelial, and tumor cell markers (Fig. 1C). The FAP$^+$Thy1$^+$ mesenchymal cell compartment could be further subdivided on the basis of PDPN expression into FAP$^+$PDPN$^+$ and FAP$^+$PDPN$^-$ populations (Fig. 1C). Both the PDPN$^+$ and PDPN$^-$ fractions of FAP$^+$ stroma were present in tumors as soon as tumor nodules were palpable ($\sim$75 mm^3), and their frequency remained constant throughout tumor progression (Supplementary Fig. S1B and S1C). Additionally, both populations were observed in multiple syngeneic tumor models, including skin, breast, lung, and gastrointestinal carcinomas (Fig. 1D). FAP$^+$PDPN$^+$ and FAP$^+$PDPN$^-$ stromal cell populations were particularly abundant in tumors with dense ECM, such as 4T1, which is a poorly immunogenic murine tumor that closely resembles human triple-negative breast carcinoma (29, 30). Therefore, we focused on this model for further analyses.

PDPN expression distinguishes between CAFs and pericytes within FAP$^+$ stroma

To further characterize the FAP$^+$ mesenchymal cells, transcriptional profiling was performed on the two FAP$^+$ tumor stromal populations (Fig. 2A), using PDPN$^+$ fibroblasts from healthy skin as a comparison population for the tissue where the tumor was located (Fig. 2B). Stromal cells were extracted from established s.c. 4T1 tumors or healthy skin and sorted to greater than 95% purity (Fig. 2C) with good sample-to-sample reproducibility (Supplementary Fig. S1D). Following standards and quality control pipelines of the Immunological Genome Project Consortium (www.immgen.org), transcriptomic profiles were generated for each subset.

Controlling for a false discovery rate of 5%, 489 genes were $\geq$2-fold differentially expressed between FAP$^+$PDPN$^+$ and FAP$^+$PDPN$^-$ stromal cells. Pathway enrichment analysis (KEGG) for the top 100 differentially expressed genes revealed that FAP$^+$PDPN$^+$ cells were characterized by expression of genes predictive of pathways associated with fibroblasts, including proteoglycan biology, WNT signaling, focal adhesions, and complement activation (Fig. 2D). On the other hand, FAP$^+$PDPN$^-$ stromal cells were enriched for pathways related to cGMP and cAMP signaling, as well as muscle contraction (Fig. 2D). Given that these pathways are associated with regulation of vascular tone (31), we hypothesized that FAP$^+$PDPN$^-$ stromal cells represent a fraction of FAP$^+$ pericytes, rather than fibroblasts, in the tumor microenvironment. To test this hypothesis, we compiled a list of fibroblast- and pericyte-specific genes based on several published papers (5, 7, 32, 33), and analyzed their expression in tumor stromal cells. This analysis revealed high expression of fibroblast markers in FAP$^+$PDPN$^+$ stromal cells, including *Dcn*, *Lox*, and *Loxl1* (Fig. 2E), as also depicted in skin fibroblasts and LN FRCs, underscoring their common lineage. FAP$^+$PDPN$^-$ stroma exhibited pronounced expression of genes previously attributed to pericytes, including *Des*, *Rgs4*, *Rgs5*, and the transcription factor *Notch 3* (refs. 5, 34; Fig. 2F). In addition, their expression pattern resembled that of primary pericytes from LNs (IAPs, integrin alpha7$^+$ pericytes; ref. 35), strengthening the argument that PDPN$^-$ tumor stromal cells represent a population of perivascular cells in tumors.

Further analysis of signature genes associated with different LN resident stromal cells also revealed similarities between PDPN$^+$ tumor stromal cells and LN FRCs, including expression of *Fap*, *Acta2*, and *Cdh11*, genes associated with activation and myofibroblast differentiation (Fig. 3A). On the other hand, PDPN$^-$ tumor stromal cells and LN IAPs shared expression of signature genes associated with pericytes (Fig. 3A). Examination of global relationships between PDPN$^+$ and PDPN$^-$ tumor stromal cells through principal component analysis reinforced their functional divergence, as depicted by their separation on principal components 1 and 2 (Fig. 3B). However, both subsets of FAP$^+$ tumor stromal cells were positioned closer to one another than to their LN counterparts (Fig. 3B), suggesting the existence of distinct transcriptomic programs in fibroblasts from different locations, likely dictated by tissue-specific environmental cues.

Morphologic examination of cytoskeletal organization in FAP$^+$ stroma from 4T1 tumors also highlighted distinct features of the

Figure 3.

PDPN$^+$ cells are CAFs and PDPN$^-$ cells are CAPs. **A,** Heat map depicting expression of canonical LN stromal genes in sorted populations. (Skin Fib, skin fibroblasts; Tum PDPN$^+$, tumor FAP$^+$PDPN$^+$ stroma; LN FRCs, lymph node fibroblastic reticular cells; Tum PDPN$^-$, tumor FAP$^+$PDPN$^-$ stroma; LN IAPs, lymph node integrin α7$^+$pericytes; LN LECs, lymph node lymphatic endothelial cells; LN BECs, lymph node blood endothelial cells.) Values were normalized, row mean centered, and $\log_2$ transformed. **B,** Principal component analysis of skin, tumor, and LN stromal cells. **C** and **D,** Cryopreserved s.c. 4T1 tumors were stained with Dapi and with antibodies against FAP and PDPN (**C**, scale bar = 40 μm) or with antibodies against FAP, PDPN, and integrin α7 (Itgα7; **D**, scale bar = 20 μm). Images are representative of >5 independent samples. **E,** Histograms showing expression of the indicated markers in freshly isolated FAP$^+$PDPN$^+$ (red) and FAP$^+$PDPN$^-$ (green) stromal cells from 4T1 tumors, as compared with isotype controls (gray). $N = 3$ independent experiments. **F,** Human breast carcinomas were digested and analyzed by FACS for the indicated markers. **G,** Histogram depicting staining for CD140α in PDPN$^+$ (red) and PDPN$^-$ (green) FAP$^+$ stromal cells from human breast carcinomas, as compared with isotype control (gray). $N = 3$ independent experiments.

two subsets. Specifically, when plated directly after sorting, PDPN$^+$ stromal cells possessed numerous protrusions, with cytoskeletal structures emblematic of myofibroblasts, such as stress fibers and supermature focal adhesions (i.e., >8 μm; Supplementary Fig. S1E). *In vivo*, FAP$^+$ PDPN$^+$ stromal cells also presented a fibroblast-like shape, with elongated cell bodies (Fig. 3C). Conversely, PDPN$^-$ tumor stromal cells cultured *in vitro* exhibited membrane ruffles (Supplementary Fig. S1F), characteristic of contractile cells. Additionally, confocal microscopic analysis of 4T1 cryosections revealed perivascular localization of FAP$^+$ PDPN$^-$ stromal cells, as well as expression of integrin α7, a marker of LN pericytes (Fig. 3D).

Differential expression of fibroblast- and pericyte-specific proteins among FAP$^+$ tumor stroma was confirmed by flow cytometry. Expression of CD140α and cadherin-11, both fibroblast markers, was restricted to PDPN$^+$ tumor stroma, whereas integrin α7 was expressed only by the PDPN$^-$ subset (Fig. 3E). In addition, these two subsets expressed both αSMA and CD140β. These two populations of FAP$^+$ mesenchymal cells were also observed in primary human breast carcinomas (Fig. 3F; Supplementary Fig. S1G). Similar to murine tumor stromal cells, both of these FAP$^+$ populations in human tumors also expressed αSMA and CD140β (Supplementary Fig. S1H). Only the subset expressing both FAP and PDPN exhibited fibroblastic markers such as CD140α (Fig. 3G) and CD44 (Supplementary Fig. S1H). Together, these results demonstrate that FAP is expressed not only by PDPN$^+$ CD140α$^+$ cadherin-11$^+$ CAFs (hereafter referred to as PDPN$^+$ CAFs) but also by PDPN$^-$ CD140α$^-$ ITGα7$^+$ pericytes (hereafter referred to as PDPN$^-$ CAPs) in both mouse and human tumors.

Distinct contributions of CAFs and CAPs to the matrix architecture of tumors

The discovery that only a subset of FAP$^+$ mesenchymal cells possessed features of fibroblasts prompted us to conduct a deeper analysis of the fibrotic potential of FAP$^+$ cells in the tumor microenvironment. Analysis across multiple stromal cells from tumors and healthy tissues revealed a fibrotic potential in PDPN$^+$ CAFs, as depicted by expression of many collagen species, including type I collagen and collagen III, expression of other fibrillar collagen genes (collagen V), and fibril-associated collagens (collagen XIV), as shown in Supplementary Fig. S2A. PDPN$^+$ CAFs also expressed many genes encoding metalloproteinases, metallopeptidases, and other ECM modifying molecules, including *Dcn* and *Fmod*, suggesting that PDPN$^+$ CAFs facilitate collagen fibrillogenesis and matrix remodeling in the tumor microenvironment. Some ECM molecules associated with poor prognosis in patients, such as *Lox*, *Loxl1*, *Tnc*, and *Postn* (5–7), were also expressed in PDPN$^+$ CAFs (Supplementary Fig. S2A).

PDPN$^-$ pericytes also expressed collagen genes, including *Col18a1*, *Col4a1*, and *Col4a2*, as well as ECM-related genes such as *Bgn* and *Postn* (Supplementary Fig. S2A), indicating that these cells likely participate in ECM remodeling around vessels. Nonetheless, a comparative analysis of ECM-related signatures in PDPN$^+$ CAFs and PDPN$^-$ CAPs indicated that, overall, the CAFs had significantly higher expression scores of these gene sets (Supplementary Fig. S2B), suggesting that PDPN$^+$ CAFs possess greater fibrotic and ECM remodeling potential, as also highlighted by their localization adjacent to and overlapping with matrix fibers (Supplementary Fig. S3). The increased expression of ECM genes in PDPN$^+$ CAFs was not merely a result of their fibroblastic nature. Genes associated with fibroblast activation and fibrosis were enriched in PDPN$^+$ CAFs as compared not only with PDPN$^-$ CAPs but also with other fibroblast populations, suggesting that the inflammatory environment of tumors promotes expression of fibrosis-related genes (Fig. 4A and B).

Given that TGFβ drives fibrosis in various pathologic conditions, and TGFβ signaling in CAFs has been associated with metastatic dissemination (33) and poor response to immunotherapy (36, 37), it is conceivable that increased fibrotic potential of fibroblasts in tumors may stem from increased TGFβ signaling. Indeed, expression of an array of TGFβ-responsive genes was significantly higher in PDPN$^+$ CAFs, as compared with PDPN$^-$ CAPs from the same tumor, fibroblasts from skin, and LN FRCs (Fig. 4C and D). Additionally, both CAPs and CAFs exhibited increased expression of TGFβ isoforms relative to nontumor fibroblasts (Fig. 4E and F). These data suggest that high TGFβ concentrations in the tumor microenvironment and increased TGFβ signaling in PDPN$^+$ CAFs may prompt ECM deposition. Indeed, PDPN$^+$ CAFs were associated with a reticular network of matrix fibers (Fig. 4G). The fact that PDPN$^-$ CAPs express TGFβ isoforms and some of TGFβ response genes suggests TGFβ signaling is active in pericytes as well, perhaps modulating their association with endothelial cells and vessel permeability (38).

Together, these data suggest that all FAP$^+$ stromal cells express an array of ECM and ECM remodeling genes and possess fibrotic potential. However, of the two FAP$^+$ stromal populations identified here, PDPN$^+$ CAFs likely dominate in shaping the matrix architecture surrounding tumors in response to profibrotic signals such as TGFβ.

T cells interact closely with CAFs in tumor periphery

The localization of T cells in tumors is influenced by the matrix architecture (39). Therefore, we sought to determine whether T cells interact with PDPN$^+$ CAFs. To this end, cryopreserved, subcutaneously grown 4T1 tumors were serially sectioned into thick (100 μm) slices, stained, and imaged by multiphoton microscopy, and individual *z*-planes were stitched together to create a single 3D reconstructed image (Fig. 5A and B). Collagen structures were visualized with second harmonic generation, PDPN$^+$ CAFs were detected with an antibody against PDPN, and immune cells were visualized with CD45 staining.

3D reconstruction of these 4T1 tumors revealed an immune-excluded phenotype characterized by a dense fibroblast/ECM structure surrounding the tumor and the presence of most tumor-infiltrating leukocytes in this region, with fewer immune cells deeper in the tumor parenchyma (Fig. 5C and D). Preferential localization of tumor-infiltrating leukocytes in stroma- and collagen-rich regions was also observed in several other murine syngeneic tumor models (Supplementary Fig. S4A–S4C). Further analysis of these stromal regions in murine tumors revealed interactions between tumor-infiltrating T cells and PDPN$^+$ CAFs and collagen fibers, with the majority of CD8$^+$ T cells establishing direct contact with fibroblasts and surrounding matrix (Fig. 5E; Supplementary Fig. S5A–S5C).

Altogether, these findings suggest that dense ECM generated by cancer-associated stromal cells may directly influence the localization of tumor-infiltrating immune cells. Furthermore,

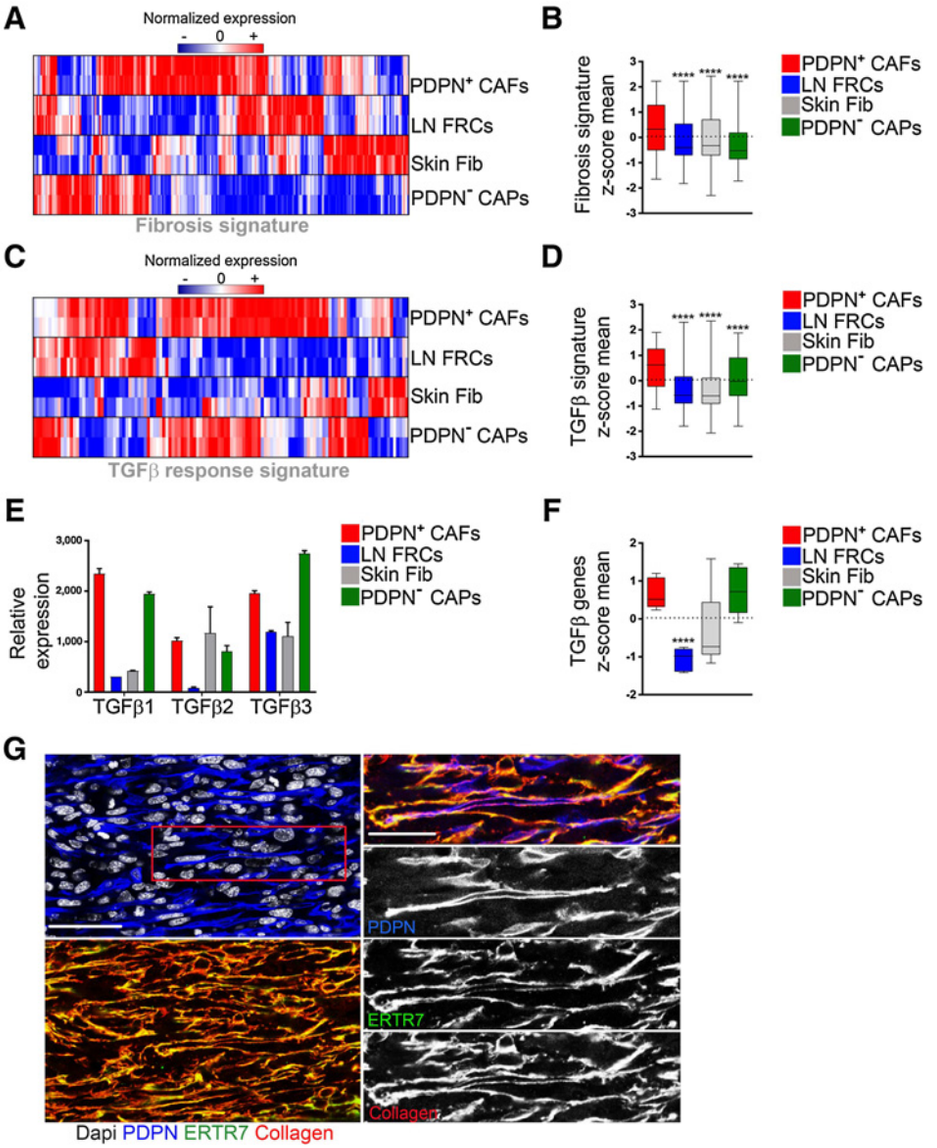

Figure 4.

PDPN$^+$ CAFs possess high fibrotic potential. **A,** Unbiased hierarchical clustering of 251 genes associated with fibrosis in PDPN$^+$ CAFs, PDPN$^-$ CAPs, FRCs, and skin fibroblasts (EV>120 for at least one population). Values were normalized, row mean centered, and $\log_2$ transformed. (Skin Fib, skin fibroblasts; LN FRCs, lymph node fibroblastic reticular cells; PDPN$^+$ CAFs, cancer-associated fibroblasts; PDPN$^-$ CAPs, cancer-associated pericytes). **B,** Z-score means of genes depicted in **A**. **C** and **D,** Heat map (**C**) and Z-scores (**D**) of 122 TGFβ-responsive genes expressed by the same populations as in **A**. **E** and **F,** Graphs depicting the expression levels of TGFβ isoforms (**E**) and the z-scores (**F**) across four cell populations. Whiskers in box plots extend to minimum and maximum values. Statistically significant differences are depicted (****, $P < 0.0001$, unpaired Student *t* test). **G,** Cryopreserved 4T1 tumors were sectioned and stained with Dapi and antibodies against PDPN, ERTR7, and collagen I. Scale bar, 50 μm. Insets show an enlargement of the boxed area. Scale bar, 30 μm. Images are representative of >5 independent samples.

close interactions observed between PDPN$^+$ CAFs and T cells raise the possibility that CAFs influence not only migration but also function of tumor-infiltrating lymphocytes. This enrichment of immune cells in peritumoral stromal-dense areas has also been observed in patients with cancer and has been suggested to curtail clinical benefits of immunotherapies (36, 37, 40). These findings raise the possibility that tumor cells co-opt tissue fibroblasts to generate a specialized architecture that collects tumor-infiltrating immune cells and impedes proper function of CD8$^+$ T lymphocytes.

PDPN$^+$ CAFs express a functional gene signature resembling that of immunosuppressive FRCs

The interactions observed between PDPN$^+$ CAFs and lymphocytes in the tumor microenvironment resembled the FRC–immune cell interplay characteristic of lymphoid organs, prompting us to explore whether PDPN$^+$ CAFs share some functional properties with LN FRCs. PDPN$^+$ CAFs did not express *Ccl19*, *Ccl21*, *Cxcl12*, or *Cxcl13*, chemokines expressed by FRCs and involved in the recruitment of naïve lymphocytes (refs. 24, 41; Fig. 6A). On the other hand, PDPN$^+$ CAFs and PDPN$^-$ CAPs were poised to support the influx of antigen-experienced T cells, as evidenced by their expression of the CXCR3 ligands *Cxcl9*, *Cxcl10*, and *Cxcl11* (Fig. 6B), in addition to other immune-relevant chemokines (Supplementary Fig. S6). Genes implicated in the survival of naïve B and T cells, namely, *Il7* and *Tnfsf13b*, were also not expressed by PDPN$^+$ CAFs, PDPN$^-$ CAPs, or skin fibroblasts (Fig. 6C). Thus, FRCs appear to be unique in their ability to support naïve lymphocytes.

On the other hand, PDPN$^+$ CAFs expressed genes associated with the induction of an immunosuppressive microenvironment, including *Tgfβ* (as shown in Fig. 4E and F). One gene expressed in PDPN$^+$ CAFs, *Nos2* (Fig. 6D), was of particular interest given that NO is produced by FRCs in response to activated T cells and required for FRC-mediated suppression of these cells (42–44).

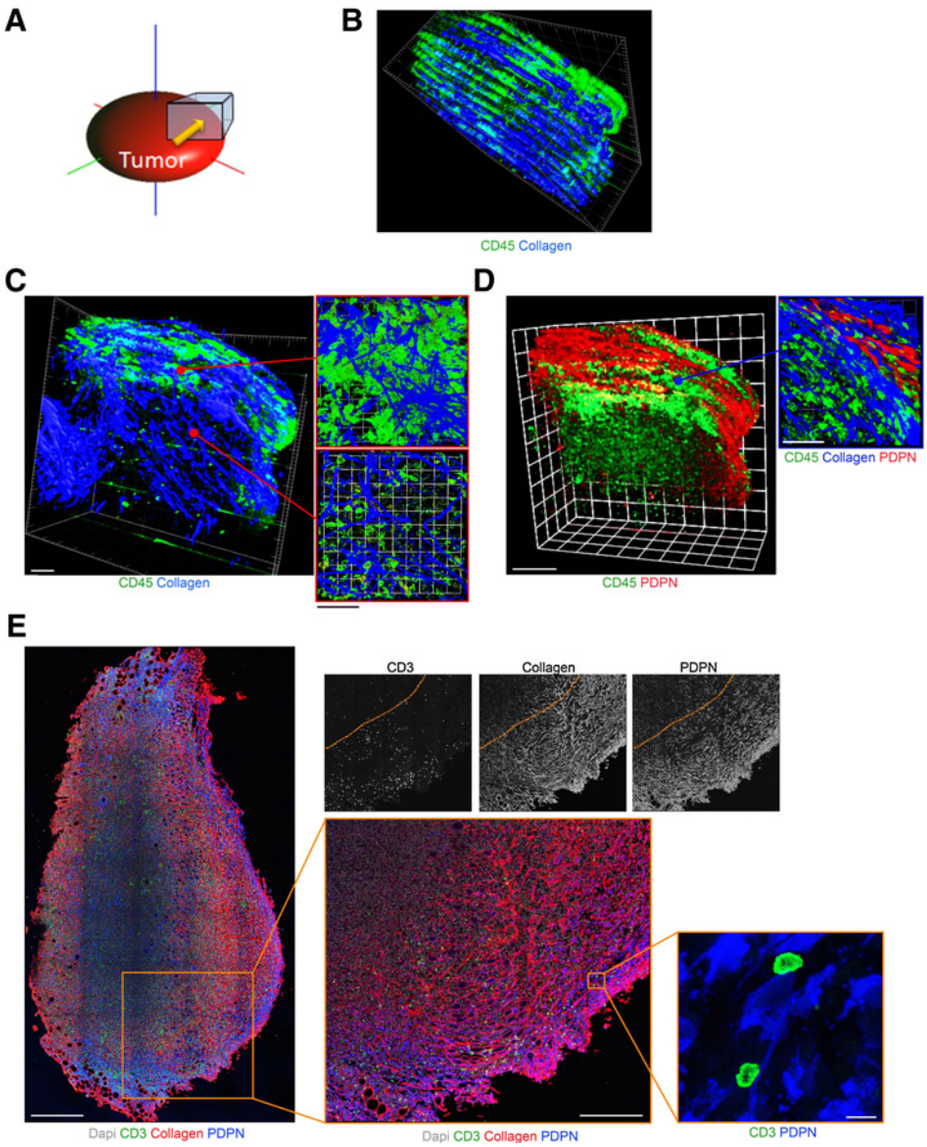

Figure 5.

T cells localize in stromal-enriched regions and interact with PDPN$^+$ CAFs. **A,** Schematic depicting the region of interest that was imaged to generate 3D visualizations of cryopreserved 4T1 tumors. **B,** To generate images, 100-μm thick tumor sections were labeled with antibodies, and tiled sections were compiled in the z-axis, resulting in a reconstructed 3D image. **C,** Cryopreserved, serial slices from s.c. 4T1 tumors generated as in **A** and **B** were stained for CD45, and images were compiled into a single image. Second harmonic generation was used to image fibrillar collagen. Scale bar, 70 μm (insets, 60 μm). $N = 2$ independent experiments. **D,** Samples as in **A** were stained with antibodies against CD45 and PDPN, imaged together with second harmonic generation signal. Scale bar, 100 μm (inset, 60 μm). $N = 2$ independent experiments. **E,** Cryopreserved s.c. 4T1 tumors were stained with Dapi and with antibodies against CD3, collagen I, and PDPN. Scale bar, 500 μm. Insets depict the close interaction between T cells and the fibroblast network. Scale bar, 250 μm and 10 μm. Dotted lines demarcate the stromal–tumor border. Images are representative of >5 independent experiments.

When examined directly *ex vivo*, *Nos2* was expressed by PDPN$^+$ CAFs, but was not detectable in resting FRCs, PDPN$^-$ CAPs, or skin fibroblasts (Fig. 6D). *Nos2* expression in CAFs was validated at the protein level. Using confocal imaging, iNOS protein was detected in PDPN$^+$ CAFs from cryopreserved s.c. 4T1 tumor tissues (Fig. 6E). Additionally, flow cytometry analysis of freshly isolated tumor stroma cells further demonstrated that expression of iNOS in FAP$^+$ stromal cells was restricted to PDPN$^+$ CAFs, as no iNOS protein was detected in PDPN$^-$ CAPs (Fig. 6F). Finally, CAFs produced NO when cocultured with activated splenocytes. This observation is in line with our previous data indicating that IFNγ and TNFα produced by activated splenocytes cause an upregulation of *iNOS* and NO in FRCs (35, 43). In contrast, NO was not detected in the supernatant of PDPN$^-$ CAPs cultured in the same conditions, consistent with their lack of *Nos2* RNA and iNOS protein (Fig. 6G). Together, these data support the hypothesis that interactions between PDPN$^+$ CAFs and tumor-infiltrating lymphocytes in the inflammatory tumor microenvironment promotes NO production by PDPN$^+$ CAFs and may lead to immunosuppression.

PDPN$^+$ CAFs restrain proliferation of activated T cells

To evaluate the functional consequences of NO produced by CAFs and the interactions between CAFs and lymphocytes in the tumor microenvironment, PDPN$^+$ CAFs were isolated from 4T1 tumors and cocultured with splenocytes *in vitro*, in the presence of anti-CD3 and anti-CD28. The proliferation of both CD4$^+$ and CD8$^+$ T cells was significantly dampened in the presence of PDPN$^+$ CAFs (Fig. 7A; Supplementary Fig. S7A), whereas early T-cell activation remained unperturbed, as indicated by increased expression of CD69 and CD25 and downregulation of CD62L (Fig. 7B). This pattern is similar to what we and others previously reported for FRCs in contact with activated T cells (42–44). These findings were recapitulated with PDPN$^+$ CAFs derived from human breast carcinomas. Briefly, human FAP$^+$PDPN$^+$ CAFs (Supplementary Fig. S7B)

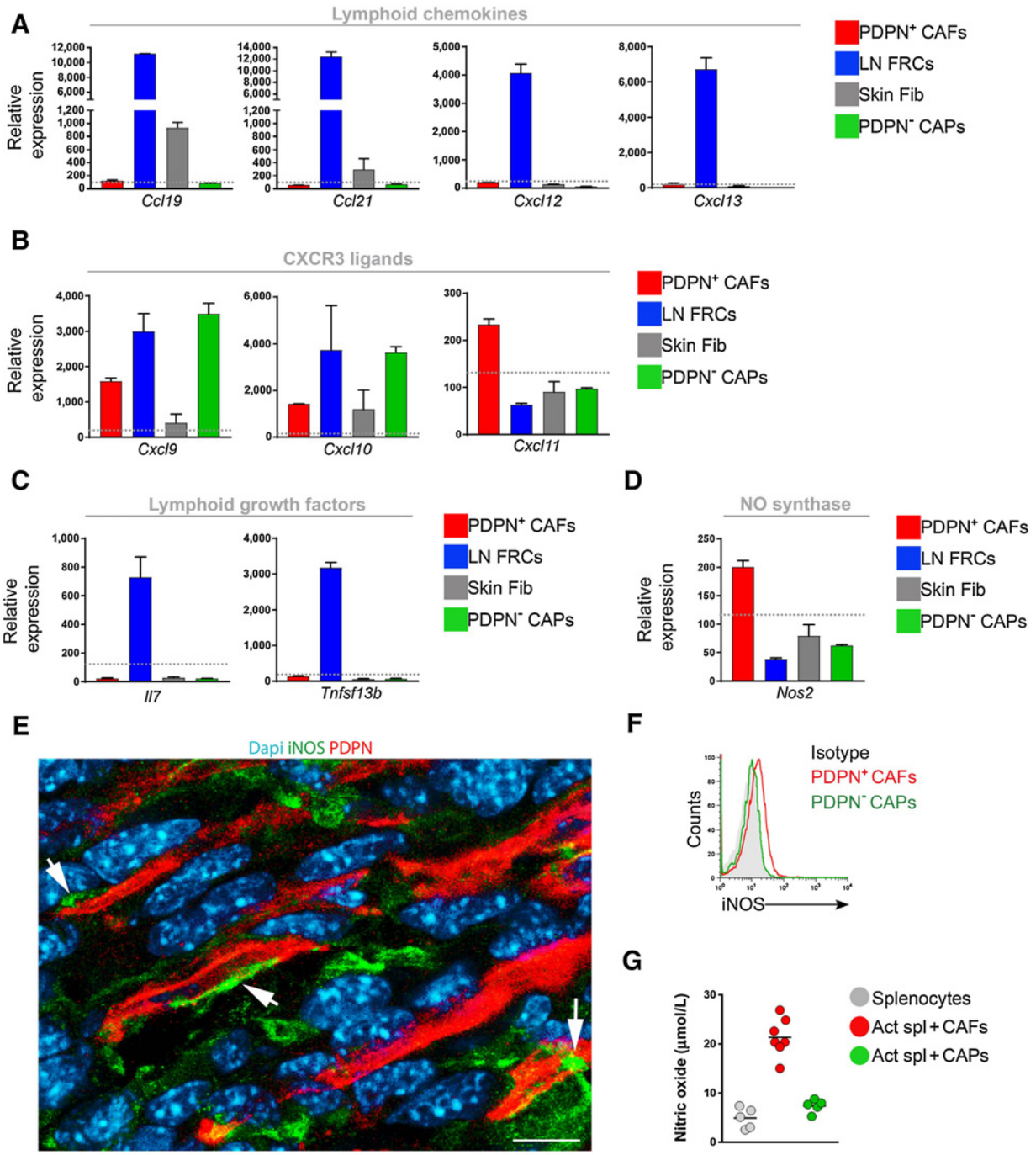

Figure 6.

Expression of immunoregulatory molecules by tumor stromal cells. **A–D,** Mean expression values from independent replicates of CAFs, FRCs, skin fibroblasts, and CAPs for lymphoid chemokines (**A**), CXCR3 ligands (**B**), cytokines (**C**), and *Nos2* (**D**). Dotted line indicates the cutoff for expression (EV = 120). **E,** Cryopreserved 4T1 tumors were sectioned and stained with Dapi and with antibodies against iNOS and PDPN. $N = 2$ independent experiments. **F,** Histogram indicating the expression of iNOS in freshly isolated $PDPN^+$ CAFs (red) and $PDPN^-$ CAPs (green), compared with isotype control (gray). $N = 2$ independent experiments. **G,** NO levels in supernatants of splenocytes alone (negative control) and $PDPN^+$ CAFs or $PDPN^-$ CAPs cultured with activated splenocytes. $N = 5$ independent experiments.

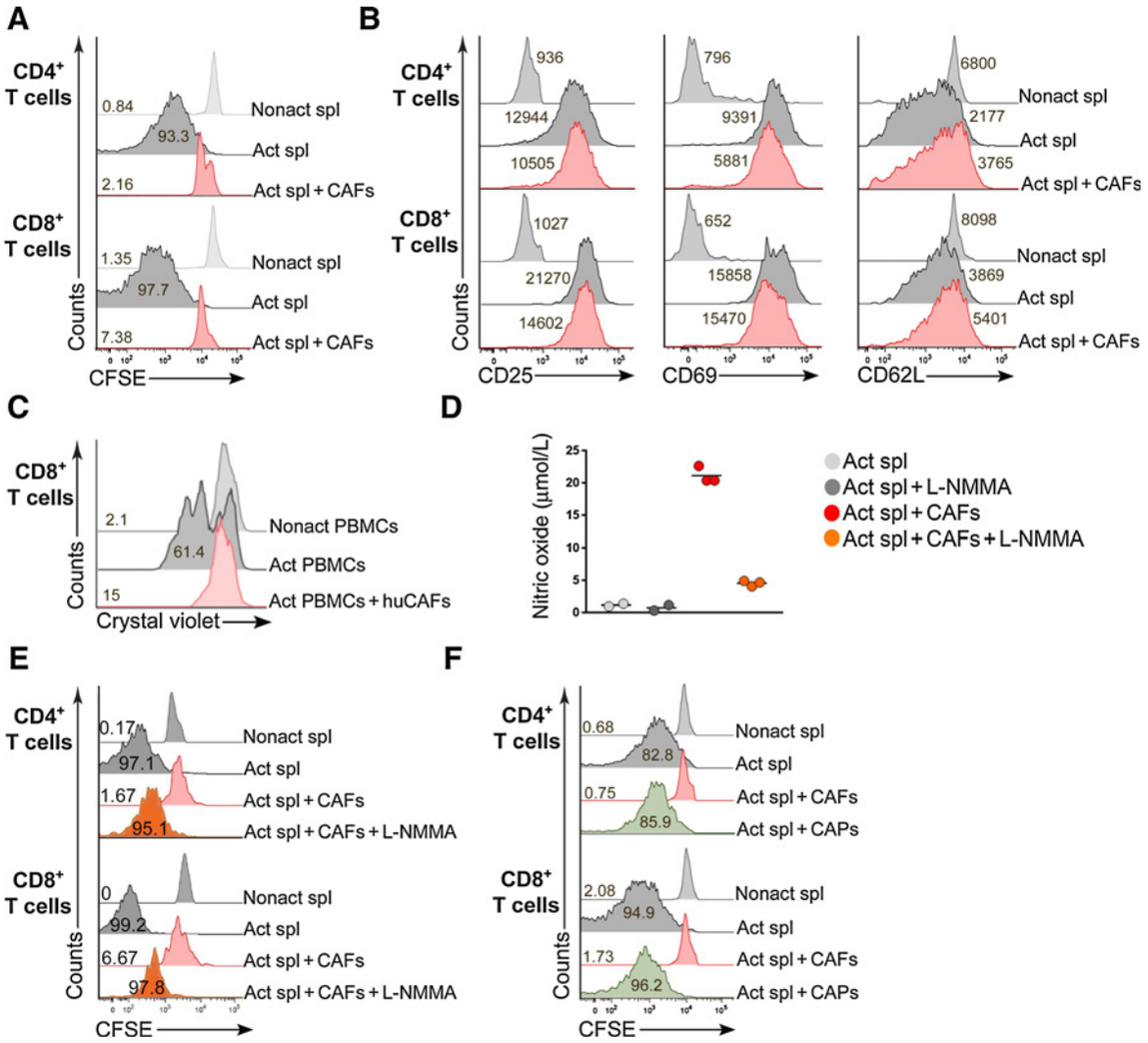

Figure 7.

PDPN$^+$ CAFs suppress the proliferation of activated T cells through the production of NO. **A,** CFSE profiles of CD4$^+$ or CD8$^+$ T cells from cultures of nonactivated splenocytes (Nonact spl) and splenocytes activated for 72 hours with anti-CD3/CD28 in the absence (Act spl) or presence of PDPN$^+$ CAFs (Act spl + CAFs). Numbers indicate the percentage of divided cells. $N = 5$ independent experiments. **B,** Expression of CD25, CD69, and CD62L on T cells cultured as in **A** for 24 hours. Numbers indicate MFI. **C,** Proliferation profile of crystal violet-labeled CD8$^+$ T cells from human PBMCs that were not activated (Nonact PBMCs), activated alone (Act PBMCs) or activated in the presence of human CAFs (Act PBMCs + huCAFs). Numbers indicate the percentage of divided cells. $N = 4$ independent experiments. **D,** NO levels produced by activated splenocytes (Act spl) cultured with L-NMMA (Act spl + L-NMMA) or with CAFs (Act spl + CAFs, Act spl + CAFs + L-NMMA). $N = 3$ independent experiments. **E,** CFSE profiles of CD4$^+$ or CD8$^+$ T cells from cultures of nonactivated splenocytes (Nonact spl), splenocytes activated alone for 72 hours (Act spl) and splenocytes activated together with PDPN$^+$ CAFs that were untreated (Act spl+CAFs) or treated with L-NMMA (Act spl + CAFs + L-NMMA). Numbers indicate the percentage of divided cells. $N = 4$ independent experiments. **F,** CFSE profiles of CD4$^+$ or CD8$^+$ T cells from cultures of nonactivated splenocytes (Nonact spl) and splenocytes activated for 72 hours in the absence (Act spl) or presence of PDPN$^+$ CAFs (Act spl + CAFs) or PDPN$^-$ CAPs (Act spl + CAPs) from the same 4T1 tumors. Numbers indicate the percentage of divided cells. $N = 4$ independent experiments.

were cultured together with human PBMCs in the presence of anti-CD3, and T-cell proliferation was subsequently measured. Consistent with mouse CAFs, the proliferation of human CD4$^+$ and CD8$^+$ T cells was almost entirely abrogated in the presence of human PDPN$^+$ CAFs (Fig. 7C; Supplementary Fig. S7C), suggesting a common immunosuppressive capability of PDPN$^+$ CAFs across species.

To assess whether fibroblast-mediated immunosuppression was mediated by the release of NO from PDPN$^+$ CAFs, we blocked NO production using N^G-Monomethyl-L-arginine, monoacetate salt (L-NMMA), a cell-permeable inhibitor of NO synthase. Consistent with our hypothesis, addition of L-NMMA was sufficient to abate NO production by PDPN$^+$ CAFs and rescue proliferation of T cells (Fig. 7D and E), pointing to a role for NO in restraining the expansion of activated T cells *in vitro*. L-NMMA had no effect on splenocytes cultured alone (Supplementary Fig. S7D), supporting the notion that reversal of suppression was due to an effect of drug on PDPN$^+$ CAFs. Additionally, despite high TGFβ expression observed in CAFs, TGFβ neutralization in the splenocyte-CAF coculture did not affect the suppressive potential of CAFs

(Supplementary Fig. S7E). Lastly, as predicted by their absence of *Nos2* expression and NO production, PDPN$^-$ CAPs did not affect the proliferation of lymphocytes (Fig. 7F), and no changes were observed upon L-NMMA addition to splenocytes cultures with CAPs (Supplementary Fig. S7F).

Collectively, these data highlight the phenotypic, functional, and spatial heterogeneity in FAP$^+$ tumor stromal cells, identifying two distinct subsets with characteristics of fibroblasts and pericytes (Supplementary Fig. S8). Additionally, this study suggests that the NO axis may represent one of the mechanisms governing CAF-mediated T-cell suppression in the tumor microenvironment.

Discussion

Stromal cells within the tumor microenvironment can promote cancer growth, progression, chemoresistance, and even immunosuppression (5, 45, 46); however, the precise composition and function of tumor stroma remain unclear. In this study, we identified two discrete populations of FAP$^+$ mesenchymal cells in mouse and human breast tumors. FAP was expressed on the surface of CAFs and CAPs, whereas PDPN expression was restricted to CAFs. The breast tumor CAFs shared some functional attributes with LN FRCs, including production of reticular fibers supporting stromal–immune cell interactions and inhibition of T-cell proliferation through NO production. In contrast, CAPs did not produce NO and had no effect on T-cell proliferation. Although these results suggest that CAPs are not immunosuppressive, we cannot exclude that under certain conditions, they may influence the function of other immune cells in the tumor microenvironment.

Our study highlighted some resemblance between CAFs and FRCs, including expression of FAP and PDPN, and myofibroblast-like characteristics. In LNs, FRCs construct a microarchitecture that facilitates interactions between immune cells, conduit function, vascular support, and the initiation of immune responses (23). Analysis of the CAF-associated matrix architecture across multiple mouse tumors illuminated a dense reticular framework, with prominent staining for ERTR7 and various collagens. Notably, tumor-infiltrating immune cells, particularly CD8$^+$ T cells, were more closely associated with CAFs and their matrix fibers than with the epithelial compartment of the tumor. Why CD8 T cells accumulate in the CAF-rich peritumoral compartment rather than in the tumor bed remains unclear. It has been suggested that "immune-exclusion" derives from a matrix-based physical barrier limiting T-cell infiltration of the tumor bed (39, 47, 48). However, chemotactic gradients and matrix scaffolding may also account for this phenotype. Indeed, both CAFs and CAPs produced several chemokines, including *Cxcl9*, *Cxcl10*, and *Cxcl11*, which could attract CXCR3$^+$ T cells entering the tumor bed.

Beyond organizing the peritumoral localization of immune cells, mouse and human CAFs exhibited immunosuppressive potential by inhibiting the proliferation of activated T cells. Bone marrow stroma and synovial fibroblasts possess immunosuppressive ability, and prostaglandin E2, TGFβ, and IL10 have been linked to this function (49–52). However, our study suggests that NO underlies the inhibitory effect of PDPN$^+$ CAFs in mouse breast tumors.

Mechanistically, NO may alter T-cell function through protein modifications, via either s-nitrosylation or peroxynitrite activity (53). In the tumor microenvironment, NO produced by myeloid cells has been associated with formation of peroxynitrite, leading to nitration of the T-cell receptor and desensitization (54). NO released by PDPN$^+$ CAFs may have similar repercussions in neighboring T cells. Additionally, nitration of chemokines, particularly CCL2, has been associated with trapping of tumor-specific T cells in peritumoral stroma. Thus, NO production by CAFs may also hinder T-cell infiltration through NO production (55). The capacity of CAFs to produce NO and suppress T-cell proliferation points to some resemblance between PDPN$^+$ CAFs and FRCs; indeed, during inflammatory conditions, FRCs acquire immunosuppressive potential, dampening the expansion of the activated T-cell pool (42–44).

Despite these similarities, FRCs exhibited unique features compared with CAFs, such as expression of chemokines and growth factors that guide and nurture naïve lymphocytes, including CCR7 ligands and *Il7*. In LNs, the drainage of tumor-derived material is sufficient to reprogram FRCs and downregulate these factors (56). Many of the transcriptional changes that occur in FRCs in tumor-draining LNs were reflected in our analysis of PDPN$^+$ CAFs. For example, we detected high expression of genes associated with fibroblast activation, such as *Acta2*, *Thy1*, and *Pdpn*, together with greater fibrotic potential, whereas *Ccl19*, *Ccl21*, *Tnfsf13b*, and *Il7* were not expressed. Consistent with previous studies, our data support the idea that the tumor milieu programs the function of tissue-resident fibroblasts, converting at least some local fibroblasts into CAFs (57, 58).

Going forward, genetic and pharmacologic efforts to manipulate tumor stromal cells using FAP-based approaches will need to be carefully considered given that this molecule can be expressed by at least two mesenchymal cell populations with dissimilar functions. Given that pericytes have been associated with a variety of functions in the tumor microenvironment (59–64), the influence of CAPs on tumor progression and antitumor immunity remains to be determined. High dimensional analysis of stromal heterogeneity across different cancer types and treatments will be crucial for understanding the diverse functions played by cell populations within this compartment and how to target them for new therapeutic approaches.

Disclosure of Potential Conflicts of Interest

J.L. Astarita is a senior scientist at Spotlight Therapeutics. G. Dranoff is Global Head, Exploratory Immuno-oncology at Novartis. No potential conflicts of interest were disclosed by the other authors.

Authors' Contributions

Conception and design: V. Cremasco, J.L. Astarita, S. Keerthivasan, M.C. Woodruff, S.J. Turley

Development of methodology: V. Cremasco, A.L. Grauel, S. Keerthivasan, E. Pure, S.J. Turley

Acquisition of data (provided animals, acquired and managed patients, provided facilities, etc.): V. Cremasco, J.L. Astarita, A.L. Grauel, M.C. Woodruff, M. Wu, L. Spel, S. Santoro, Z. Amoozgar, T. Laszewski, S. Cruz Migoni, K. Knoblich, A.L. Fletcher, M. LaFleur

Analysis and interpretation of data (e.g., statistical analysis, biostatistics, computational analysis): V. Cremasco, J.L. Astarita, A.L. Grauel, S. Keerthivasan, K. MacIsaac, M.C. Woodruff, M. Wu, S. Santoro, Z. Amoozgar, S. Cruz Migoni, A.L. Fletcher, K.W. Wucherpfennig, S.J. Turley

Writing, review, and/or revision of the manuscript: V. Cremasco, J.L. Astarita, A.L. Grauel, S. Keerthivasan, Z. Amoozgar, K.W. Wucherpfennig, E. Pure, G. Dranoff, S.J. Turley

Administrative, technical, or material support (i.e., reporting or organizing data, constructing databases): V. Cremasco, A.L. Grauel

Study supervision: V. Cremasco, G. Dranoff, M.C. Carroll, S.J. Turley

Other (provided key antibody reagent that was characterized in my laboratory that provided the basis for interpreting results obtained in this study and developed methodology for its use): E. Pure

Acknowledgments

This study was supported by the NIH (5R01 DK074500-08, 2P01AI045757-15, and R21 CA182598-01 to S.J. Turley; R01 AI039246, P01 AI078897, and R37 AI054636 to M.C. Carroll; and T32 CA 070083-15 to V. Cremasco), the Barr Foundation (S.J. Turley), the American Cancer Society (S.J. Turley), the Cancer Research Institute (V. Cremasco), and the Science Foundation (S.J. Turley).

We thank Dr. Michael Brenner for the Cadherin-11 antibody and Dr. Jun Sonoda for critical reading of the manuscript.

The costs of publication of this article were defrayed in part by the payment of page charges. This article must therefore be hereby marked *advertisement* in accordance with 18 U.S.C. Section 1734 solely to indicate this fact.

Received February 17, 2018; revised July 11, 2018; accepted September 17, 2018; published first September 28, 2018.

References

1. Lai D, Ma L, Wang F. Fibroblast activation protein regulates tumor-associated fibroblasts and epithelial ovarian cancer cells. Int J Oncol 2012; 41:541–50.
2. Marsh D, Suchak K, Moutasim KA, Vallath S, Hopper C, Jerjes W, et al. Stromal features are predictive of disease mortality in oral cancer patients. J Pathol 2011;223:470–81.
3. Tsujino T, Seshimo I, Yamamoto H, Ngan CY, Ezumi K, Takemasa I, et al. Stromal myofibroblasts predict disease recurrence for colorectal cancer. Clin Cancer Res 2007;13:2082–90.
4. Yamashita M, Ogawa T, Zhang X, Hanamura N, Kashikura Y, Takamura M, et al. Role of stromal myofibroblasts in invasive breast cancer: stromal expression of alpha-smooth muscle actin correlates with worse clinical outcome. Breast Cancer 2012;19:170–6.
5. Turley SJ, Cremasco V, Astarita JL. Immunological hallmarks of stromal cells in the tumour microenvironment. Nat Rev Immunol 2015;15:669–82.
6. Kalluri R, Zeisberg M. Fibroblasts in cancer. Nat Rev Cancer 2006; 6:392–401.
7. Kalluri R. The biology and function of fibroblasts in cancer. Nat Rev Cancer 2016;16:582–98.
8. Wang LC, Lo A, Scholler J, Sun J, Majumdar RS, Kapoor V, et al. Targeting fibroblast activation protein in tumor stroma with chimeric antigen receptor T cells can inhibit tumor growth and augment host immunity without severe toxicity. Cancer Immunol Res 2014;2:154–66.
9. Lo A, Wang LS, Scholler J, Monslow J, Avery D, Newick K, et al. Tumor-promoting desmoplasia is disrupted by depleting FAP-expressing stromal cells. Cancer Res 2015;75:2800–10.
10. Lo A, Li CP, Buza EL, Blomberg R, Govindaraju P, Avery D, et al. Fibroblast activation protein augments progression and metastasis of pancreatic ductal adenocarcinoma. JCI Insight 2017;2. pii:92232.
11. Liao D, Luo Y, Markowitz D, Xiang R, Reisfeld RA. Cancer associated fibroblasts promote tumor growth and metastasis by modulating the tumor immune microenvironment in a 4T1 murine breast cancer model. PLoS One 2009;4:e7965.
12. Loeffler M, Kruger JA, Niethammer AG, Reisfeld RA. Targeting tumor-associated fibroblasts improves cancer chemotherapy by increasing intratumoral drug uptake. J Clin Invest 2006;116:1955–62.
13. Feig C, Jones JO, Kraman M, Wells RJ, Deonarine A, Chan DS, et al. Targeting CXCL12 from FAP-expressing carcinoma-associated fibroblasts synergizes with anti-PD-L1 immunotherapy in pancreatic cancer. Proc Natl Acad Sci USA 2013;110:20212–7.
14. Kraman M, Bambrough PJ, Arnold JN, Roberts EW, Magiera L, Jones JO, et al. Suppression of antitumor immunity by stromal cells expressing fibroblast activation protein-alpha. Science 2010;330: 827–30.
15. Arnold JN, Magiera L, Kraman M, Fearon DT. Tumoral immune suppression by macrophages expressing fibroblast activation protein-alpha and heme oxygenase-1. Cancer Immunol Res 2014;2:121–6.
16. Roberts EW, Deonarine A, Jones JO, Denton AE, Feig C, Lyons SK, et al. Depletion of stromal cells expressing fibroblast activation protein-alpha from skeletal muscle and bone marrow results in cachexia and anemia. J Exp Med 2013;210:1137–51.
17. Denton AE, Roberts EW, Linterman MA, Fearon DT. Fibroblastic reticular cells of the lymph node are required for retention of resting but not activated CD8+ T cells. Proc Natl Acad Sci USA 2014; 111:12139–44.
18. Cannon AR, Owen MK, Guerrero MS, Kerber ML, Goicoechea SM, Hemstreet KC, et al. Palladin expression is a conserved characteristic of the desmoplastic tumor microenvironment and contributes to altered gene expression. Cytoskeleton 2015;72:402–11.
19. Ozdemir BC, Pentcheva-Hoang T, Carstens JL, Zheng X, Wu CC, Simpson TR, et al. Depletion of carcinoma-associated fibroblasts and fibrosis induces immunosuppression and accelerates pancreas cancer with reduced survival. Cancer Cell 2014;25:719–34.
20. Rhim AD, Oberstein PE, Thomas DH, Mirek ET, Palermo CF, Sastra SA, et al. Stromal elements act to restrain, rather than support, pancreatic ductal adenocarcinoma. Cancer Cell 2014;25:735–47.
21. Ohlund D, Handly-Santana A, Biffi G, Elyada E, Almeida AS, Ponz-Sarvise M, et al. Distinct populations of inflammatory fibroblasts and myofibroblasts in pancreatic cancer. J Exp Med 2017;214:579–96.
22. Su S, Chen J, Yao H, Liu J, Yu S, Lao L, et al. CD10(+)GPR77(+) cancer-associated fibroblasts promote cancer formation and chemoresistance by sustaining cancer stemness. Cell 2018;172:841–56.e16.
23. Fletcher AL, Acton SE, Knoblich K. Lymph node fibroblastic reticular cells in health and disease. Nat Rev Immunol 2015;15:350–61.
24. Chang JE, Turley SJ. Stromal infrastructure of the lymph node and coordination of immunity. Trends Immunol 2015;36:30–9.
25. Fletcher AL, Malhotra D, Acton SE, Lukacs-Kornek V, Bellemare-Pelletier A, Curry M, et al. Reproducible isolation of lymph node stromal cells reveals site-dependent differences in fibroblastic reticular cells. Front Immunol 2011;2:35.
26. Laverman P, van der Geest T, Terry SY, Gerrits D, Walgreen B, Helsen MM, et al. Immuno-PET and immuno-SPECT of rheumatoid arthritis with radiolabeled anti-fibroblast activation protein antibody correlates with severity of arthritis. J Nucl Med 2015;56:778–83.
27. Mizoguchi F, Slowikowski K, Wei K, Marshall JL, Rao DA, Chang SK, et al. Functionally distinct disease-associated fibroblast subsets in rheumatoid arthritis. Nat Commun 2018;9:789.
28. Astarita JL, Acton SE, Turley SJ. Podoplanin: emerging functions in development, the immune system, and cancer. Front Immunol 2012; 3:283.
29. Tao K, Fang M, Alroy J, Sahagian GG. Imagable 4T1 model for the study of late stage breast cancer. BMC Cancer 2008;8:228.
30. Miller FR, Miller BE, Heppner GH. Characterization of metastatic heterogeneity among subpopulations of a single mouse mammary tumor: heterogeneity in phenotypic stability. Invasion Metastasis 1983; 3:22–31.
31. Carvajal JA, Germain AM, Huidobro-Toro JP, Weiner CP. Molecular mechanism of cGMP-mediated smooth muscle relaxation. J Cell Physiol 2000;184:409–20.
32. Kendall RT, Feghali-Bostwick CA. Fibroblasts in fibrosis: novel roles and mediators. Front Pharmacol 2014;5:123.
33. Calon A, Lonardo E, Berenguer-Llergo A, Espinet E, Hernando-Momblona X, Iglesias M, et al. Stromal gene expression defines poor-prognosis subtypes in colorectal cancer. Nat Genet 2015;47:320–9.
34. Armulik A, Genove G, Betsholtz C. Pericytes: developmental, physiological, and pathological perspectives, problems, and promises. Dev Cell 2011;21:193–215.

35. Malhotra D, Fletcher AL, Astarita J, Lukacs-Kornek V, Tayalia P, Gonzalez SF, et al. Transcriptional profiling of stroma from inflamed and resting lymph nodes defines immunological hallmarks. Nat Immunol 2012; 13:499–510.
36. Mariathasan S, Turley SJ, Nickles D, Castiglioni A, Yuen K, Wang Y, et al. TGFbeta attenuates tumour response to PD-L1 blockade by contributing to exclusion of T cells. Nature 2018;554:544–8.
37. Tauriello DVF, Palomo-Ponce S, Stork D, Berenguer-Llergo A, Badia-Ramentol J, Iglesias M, et al. TGFbeta drives immune evasion in genetically reconstituted colon cancer metastasis. Nature 2018;554:538–43.
38. Sieczkiewicz GJ, Herman IM. TGF-beta 1 signaling controls retinal pericyte contractile protein expression. Microvasc Res 2003;66:190–6.
39. Salmon H, Donnadieu E. The extracellular matrix: an obstacle to T cell-tumor cell interaction. Med Sci 2012;28:824–6.
40. Chen DS, Mellman I. Elements of cancer immunity and the cancer-immune set point. Nature 2017;541:321–30.
41. Brown FD, Turley SJ. Fibroblastic reticular cells: organization and regulation of the T lymphocyte life cycle. J Immunol 2015;194:1389–94.
42. Siegert S, Huang HY, Yang CY, Scarpellino L, Carrie L, Essex S, et al. Fibroblastic reticular cells from lymph nodes attenuate T cell expansion by producing nitric oxide. PLoS One 2011;6:e27618.
43. Lukacs-Kornek V, Malhotra D, Fletcher AL, Acton SE, Elpek KG, Tayalia P, et al. Regulated release of nitric oxide by nonhematopoietic stroma controls expansion of the activated T cell pool in lymph nodes. Nat Immunol 2011;12:1096–104.
44. Khan O, Headley M, Gerard A, Wei W, Liu L, Krummel MF. Regulation of T cell priming by lymphoid stroma. PLoS One 2011;6:e26138.
45. Quezada SA, Peggs KS, Simpson TR, Allison JP. Shifting the equilibrium in cancer immunoediting: from tumor tolerance to eradication. Immunol Rev 2011;241:104–18.
46. Hugo W, Zaretsky JM, Sun L, Song C, Moreno BH, Hu-Lieskovan S, et al. Genomic and transcriptomic features of response to anti-PD-1 therapy in metastatic melanoma. Cell 2016;165:35–44.
47. Salmon H, Franciszkiewicz K, Damotte D, Dieu-Nosjean MC, Validire P, Trautmann A, et al. Matrix architecture defines the preferential localization and migration of T cells into the stroma of human lung tumors. J Clin Invest 2012;122:899–910.
48. Jiang H, Hegde S, Knolhoff BL, Zhu Y, Herndon JM, Meyer MA, et al. Targeting focal adhesion kinase renders pancreatic cancers responsive to checkpoint immunotherapy. Nat Med 2016;22:851–60.
49. Krampera M, Glennie S, Dyson J, Scott D, Laylor R, Simpson E, et al. Bone marrow mesenchymal stem cells inhibit the response of naive and memory antigen-specific T cells to their cognate peptide. Blood 2003;101:3722–9.
50. Keating A. How do mesenchymal stromal cells suppress T cells? Cell Stem Cell 2008;2:106–8.
51. Di Nicola M, Carlo-Stella C, Magni M, Milanesi M, Longoni PD, Matteucci P, et al. Human bone marrow stromal cells suppress T-lymphocyte proliferation induced by cellular or nonspecific mitogenic stimuli. Blood 2002;99:3838–43.
52. Bartholomew A, Sturgeon C, Siatskas M, Ferrer K, McIntosh K, Patil S, et al. Mesenchymal stem cells suppress lymphocyte proliferation in vitro and prolong skin graft survival in vivo. Exp Hematol 2002;30:42–8.
53. Bogdan C. Nitric oxide synthase in innate and adaptive immunity: an update. Trends Immunol 2015;36:161–78.
54. Nagaraj S, Gupta K, Pisarev V, Kinarsky L, Sherman S, Kang L, et al. Altered recognition of antigen is a mechanism of CD8+ T cell tolerance in cancer. Nat Med 2007;13:828–35.
55. Molon B, Ugel S, Del Pozzo F, Soldani C, Zilio S, Avella D, et al. Chemokine nitration prevents intratumoral infiltration of antigen-specific T cells. J Exp Med 2011;208:1949–62.
56. Riedel A, Shorthouse D, Haas L, Hall BA, Shields J. Tumor-induced stromal reprogramming drives lymph node transformation. Nat Immunol 2016;17:1118–27.
57. Arina A, Idel C, Hyjek EM, Alegre ML, Wang Y, Bindokas VP, et al. Tumor-associated fibroblasts predominantly come from local and not circulating precursors. Proc Natl Acad Sci USA 2016;113:7551–6.
58. Cheng HW, Onder L, Cupovic J, Boesch M, Novkovic M, Pikor N, et al. CCL19-producing fibroblastic stromal cells restrain lung carcinoma growth by promoting local antitumor T cell responses. J Allergy Clin Immunol 2018. doi 10.1016/j.jaci.2017.12.998.
59. Viski C, Konig C, Kijewska M, Mogler C, Isacke CM, Augustin HG. Endosialin-expressing pericytes promote metastatic dissemination. Cancer Res 2016;76:5313–25.
60. Murgai M, Ju W, Eason M, Kline J, Beury DW, Kaczanowska S, et al. KLF4-dependent perivascular cell plasticity mediates pre-metastatic niche formation and metastasis. Nat Med 2017;23:1176–90.
61. Kim J, de Sampaio PC, Lundy DM, Peng Q, Evans KW, Sugimoto H, et al. Heterogeneous perivascular cell coverage affects breast cancer metastasis and response to chemotherapy. JCI Insight 2016;1: e90733.
62. Fabian KP, Chi-Sabins N, Taylor JL, Fecek R, Weinstein A, Storkus WJ. Therapeutic efficacy of combined vaccination against tumor pericyte-associated antigens DLK1 and DLK2 in mice. Oncoimmunology 2017;6: e1290035.
63. Cantelmo AR, Conradi LC, Brajic A, Goveia J, Kalucka J, Pircher A, et al. Inhibition of the glycolytic activator PFKFB3 in endothelium induces tumor vessel normalization, impairs metastasis, and improves chemotherapy. Cancer Cell 2016;30:968–85.
64. Ni C, Ma P, Qu L, Wu F, Hao J, Wang R, et al. Accelerated tumour metastasis due to interferon-gamma receptor-mediated dissociation of perivascular cells from blood vessels. J Pathol 2017;242:334–46.